

# FRACTIONAL VEGETATION COVER ESTIMATION FROM PROBA/CHRIS DATA: METHODS, ANALYSIS OF ANGULAR EFFECTS AND APPLICATION TO THE LAND SURFACE EMISSIVITY RETRIEVAL

J. C. Jiménez-Muñoz<sup>(1)</sup>, J. A. Sobrino<sup>(1)</sup>, L. Guanter<sup>(2)</sup>, J. Moreno<sup>(2)</sup>, A. Plaza<sup>(3)</sup> and P. Matínez<sup>(3)</sup>

<sup>(1)</sup>Global Change Unit, Faculty of Physics, University of Valencia, Burjassot (Spain), Email: [jcjm@uv.es](mailto:jcjm@uv.es), [sobrino@uv.es](mailto:sobrino@uv.es)

<sup>(2)</sup>Remote Sensing Unit – Laboratory of Earth Observation, Faculty of Physics, University of Valencia, Burjassot (Spain), Email: [luis.guanter@uv.es](mailto:luis.guanter@uv.es), [jose.moreno@uv.es](mailto:jose.moreno@uv.es)

<sup>(3)</sup>Neural Network and Signal Processing Group, Computer Science Department, University of Extremadura, Cáceres (Spain), Email: [aplaza@unex.es](mailto:aplaza@unex.es), [pablomar@unex.es](mailto:pablomar@unex.es)

## ABSTRACT/RESUME

In this paper, two different methods for fractional vegetation cover (FVC) retrieval from CHRIS (Compact High Resolution Imaging Spectrometer) data based on vegetation indices have been analyzed. The first method uses NDVI (Normalized Difference Vegetation Index) values, as suggested, among others, by Carlson and Ripley (1997) and Gutman and Ignatov (1998), and the second method uses VARI (Variable Atmospherically Resistant Index) values as suggested by Gitelson et al. (2002). In addition, a simple Spectral Mixture Analysis has been also carried out in order to obtain the fractional vegetation cover. The different methods have been tested using vegetation cover values obtained from hemispherical photographs. All methods provide differences with in situ values lower than 15%. The methods based on the VARI and the spectral mixture analysis show the best results, with differences lower than 10%. Substantial angular effects for the different view zenith angles of CHRIS acquisitions have not been found. The fractional vegetation cover has been used in order to obtain land surface emissivity maps with a very simplified approximation, which is only valid for flat surfaces because it does not take into account the cavity effect. In this way, land surface emissivity, which is a parameter used when working with thermal infrared data, can be retrieved from sensors with no available thermal bands.

## 1. INTRODUCTION

Knowledge of the biophysical characteristics of vegetation is necessary for describing energy and mass fluxes at the Earth's surface using Global Circulation Models (GCMs), water models, and carbon cycle models [1]. Fraction vegetation cover (FVC) is one of the main biophysical parameters involved in the surface processes, which is also a necessary requirement for Numerical Weather Prediction, regional and global climate modelling, and global change monitoring [2,3]. Remote sensing is an effective tool for observing the abundance, distribution and evolution of the FVC, which can be considered as an indicator of the land degradation [4].

Despite the major advances made in the field of remote sensing, the number of parameters that interact in the problem is still greater than the intrinsic dimension of the spectral data that are provided by sensors. Therefore, it is necessary to use approximate methods. Vegetation indices (VIs) and spectral mixture analysis (SMA) are the techniques most frequently used in remote sensing to estimate the FVC [5], and they have been applied in this paper to data acquired by the CHRIS (Compact High Resolution Imaging Spectrometer) instrument on board the ESA PROject for On-Board Autonomy (PROBA) platform.

The PROBA/CHRIS system, launched on the 22th October 2001, is a technology demonstration experiment to take advantage of autonomous pointing capabilities of a generic platform suitable for Earth Observation purposes. In combination, the coupled PROBA/CHRIS system [6] provides high spatial resolution hyperspectral/multiangular data, what constitutes a new generation of remote sensing information. On one hand, the PROBA platform provides pointing in both across-track and along-track directions. In this way, the PROBA/CHRIS system has multiangular capabilities, acquiring up to 5 consecutive images from 5 different view zenith angles (VZA) in one single satellite overpass. Each imaged target has an associated "fly-by" position, which is the position on the ground track when the platform zenith angle, as seen from the target, is a minimum (i.e. Minimum Zenith Angle (MZA)). On the other hand, CHRIS measures over the visible/near-infrared (NIR) bands from 400 nm to 1050 nm, with a minimum spectral sampling interval ranging between 1.25 (@400 nm) and 11 nm (@1000 nm). It can operate in different modes, thus compromising the number of spectral bands and the spatial resolution because of storage reasons.

CHRIS acquisitions at different view zenith angles have also been used in order to analyze the angular effects. Once the FVC has been retrieved, it has been used in order to provide land surface emissivity maps, which is an important parameter involved in thermal remote sensing for accurate retrieval of land surface temperature.

The paper is organized as follows. Section 2 describes the adopted analysis methodology and the CHRIS/PROBA data sets used in experiments. Section 3 provides an overview of several methods to derive FVC from the data sets above. Section 4 provides a comprehensive analysis of angular effects on the FVC estimations, while Section 5 discusses how FVC can be used to provide land surface emissivity maps. Finally, Section 6 concludes with some remarks and hints at plausible future research.

## 2. METHODOLOGY

### 2.1. PROBA/CHRIS data and the SPARC field campaigns

The PROBA/CHRIS imagery used in the validation of the methodology comes from the dedicated ESA SPARC campaign [7]. It offered a unique situation in which PROBA/CHRIS images were acquired simultaneously to in-situ atmospheric and ground measurements.

The first SPARC campaign took place in Barrax, La Mancha, Spain, from 12 to 14 of July 2003, under the umbrella of a formal ESA campaign as part of Phase-A Preparations for the SPECTRA mission. The reason for the selection of the 12-13-14 of July was the coincidence with three consecutive days of PROBA/CHRIS overpasses. The 5 acquisition angles for each of the two days are plotted in Fig. 1. Previously to the atmospheric correction, the images were geometrically corrected firstly. Afterwards, drop-outs and striping noises were corrected as well.

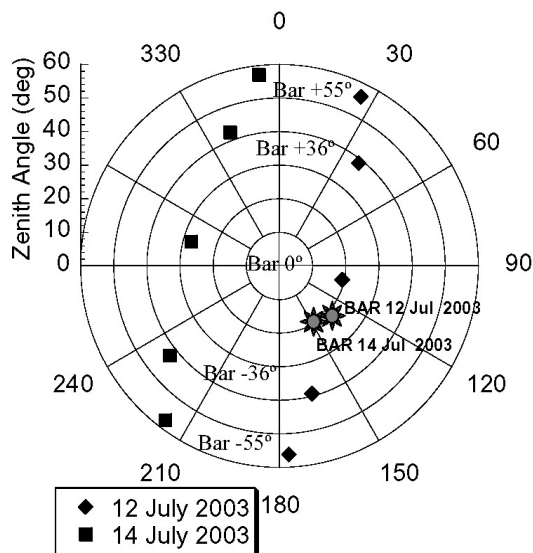


**Fig. 1.** Acquisition geometries and illumination angles for the CHRIS/PROBA images acquired over Barrax on the 12th and the 14th of July 2003.

The Barrax site is a flat continental area with an average elevation over the sea level of around 700 m. There is a big contrast in natural surfaces, ranging from green dense vegetation fields (e.g. potatoes crops) to dry bare soils. The irrigation method in the region consists of circular pivots, what results in homogeneous large circular fields easily identifiable in the image. Besides, all the crops in the site have been classified previously, so a detailed map of the area with in-situ reflectance measurements, as well as several biophysical variables, is available.

### 2.2. Atmospheric correction

Concerning the atmospheric correction, the normal procedure in the processing of hyperspectral data consists in using atmospheric correction methods lying on a radiative transfer approach. Those usually start with the retrieval of the main atmospheric parameters from the data, using sophisticated algorithms to invert the measured Top-Of-Atmosphere (TOA) radiances. The accuracy of the retrievals is strongly conditioned by the spectral calibration of the instrument, and the subsequent surface reflectance as well.

However, since the PROBA/CHRIS system was designed as a technology demonstrator, radiometric performance is somehow limited for scientific applications. For this reason, PROBA/CHRIS 2003 and 2004 data (improvements for 2005 are foreseen) presents some mis-calibration trends all over the covered spectral region [8], being the underestimation of the signal in the NIR wavelengths the most important one. As a result, common atmospheric correction methods would not lead to acceptable results. With this framework, a dedicated atmospheric correction algorithm for PROBA/CHRIS data was designed [9].

### 2.3. In situ measurements

FVC was estimated from ground measurements using an hemispherical digital camera. One of the main interest of hemispherical photographs is that the camera can be used under the canopy for upward and downward looking. Furthermore, the use of fish-eye lens allows the gap fraction to be evaluated in all viewing directions, which increases the accuracy of the derived FVC. Once properly classified, hemispherical photographs provide a detailed map of sky/soil visibility and obstruction. In turn, solar radiation regimes and canopy characteristics can be inferred from this map of sky geometry. The sampling strategy to be followed was designed according to statistical requirements. The dimension of the ESUs (Elementary Sample Unit) selected were approximately 20x20 m<sup>2</sup>, and according to statistical requirements, between 4 and 15 ESUs were necessary to fully characterize the crop. A detailed information about the spatial sampling strategy, the measuring method and

the hemispherical photograph processing can be found in [10]. Fig. 2 shows the land use map for the Barrax test site with the ESUs marked, whereas Table 1 shows the mean values and the standard deviation for the FVC measured over the different crops by using hemispherical photographs.

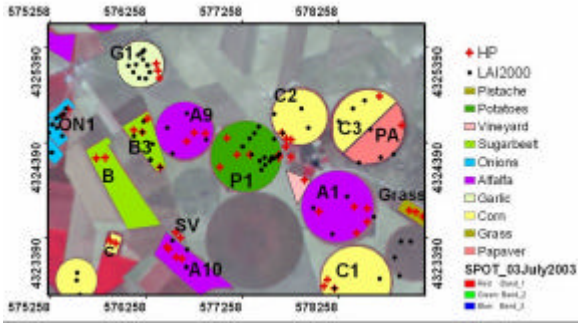


**Fig. 2.** Land use map for the Barrax test site. Red crosses indicate the points where hemispherical photographs (HP) were taken.

**Table 1.** Fractional vegetation cover measured in situ over different samples using hemispherical photographs ( $FVC_{in\ situ}$ ) and standard deviation values ( $\sigma$ ).

Sample	Notation	$FVC_{in\ situ}$	$\sigma$
Garlic	G1	0.12	0.09
Corn	C2	0.71	0.12
Corn	C1	0.63	0.08
Sugarbeet	B3	0.923	0.013
Alfalfa	A10	0.73	0.12
Alfalfa	A1	0.59	0.12
Potatoes	P1	0.96	0.04

### 3. DERIVING FVC FROM PROBA/CHRIS DATA

#### 3.1. Vegetation indices and empirical approaches

Fractional vegetation cover (FVC) has been traditionally estimated from remote sensing data using empirical relations with vegetation indices, as for example the NDVI (Normalized Difference Vegetation Index), given by

$$NDVI = \frac{\rho_{nir} - \rho_{red}}{\rho_{nir} + \rho_{red}} \quad (1)$$

where  $\rho_{nir}$  and  $\rho_{red}$  are the at-surface reflectivities obtained from sensor bands located in the near infrared (nir) and red spectral regions. PROBA/CHRIS bands 48

(centered at  $0.852 \mu m$ ) and 25 (centered at  $0.674 \mu m$ ) can be then used in order to obtain the NDVI. In order to obtain FVC, a scaled NDVI ( $NDVI^*$ ) must be defined according to:

$$NDVI^* = \frac{NDVI - NDVI_0}{NDVI_\infty - NDVI_0} \quad (2)$$

where  $NDVI_0$  and  $NDVI_\infty$  correspond to the values of NDVI for bare soil and a surface with a fractional vegetation cover of 100%, respectively. Once the scaled NDVI is defined, FVC can be obtained using a linear relationship as proposed, among others, by [11]:

$$FVC = NDVI^* \quad (3)$$

or using a square root relation as proposed, among others, by [12]:

$$FVC = NDVI^{*2} \quad (4)$$

The impact of the uncertainties on FVC estimation from NDVI values can be known by means of a sensitivity analysis. Taking into account Equation (2) and, for example, the linear relation given by Equation (3), the error on FVC,  $e(FVC)$ , will be given by:

$$e(FVC) = \sqrt{d_{NDVI}^2 + d_{NDVI_\infty}^2 + d_{NDVI_0}^2} \quad (5)$$

where

$$d_{NDVI} = \left| \frac{\partial FVC}{\partial NDVI} \right| e(NDVI) \quad (6)$$

$$d_{NDVI_\infty} = \left| \frac{\partial FVC}{\partial NDVI_\infty} \right| e(NDVI_\infty) \quad (7)$$

$$d_{NDVI_0} = \left| \frac{\partial FVC}{\partial NDVI_0} \right| e(NDVI_0) \quad (8)$$

and  $e(NDVI)$ ,  $e(NDVI_\infty)$ ,  $e(NDVI_0)$  are the errors on NDVI,  $NDVI_\infty$  and  $NDVI_0$ , respectively. Equations (5) to (8) have been applied considering the values proposed by [11],  $NDVI_0 = 0.04 \pm 0.03$  and  $NDVI_\infty = 0.52 \pm 0.03$ , and the values extracted from the ASTER spectral library,  $NDVI_0 = 0.13 \pm 0.09$  and  $NDVI_\infty = 0.801 \pm 0.012$ . A value for the error on NDVI of 0.05 has been considered. Table 2 shows the error on FVC when the values proposed by [11] are considered, with errors lower than 15%. Table 3 shows the errors

when values extracted from ASTER spectral library are considered, with errors slightly better than the previous case, lower than 12%.

**Table 2.** Errors on the fractional vegetation cover,  $e(\text{FVC})$ , depending on the NDVI value considered and obtained according to the sensibility analysis given by Equations (5) to (8). The methodology proposed by Gutmand and Ignatov (1998) has been considered.

NDVI	$d_{\text{NDVI}}$	$d_{\text{NDVI}\%}$	$d_{\text{NDVI}0}$	$e(\text{FVC})$
0.10	0.10	0.01	0.09	0.14
0.20	0.10	0.03	0.07	0.13
0.30	0.10	0.06	0.05	0.13
0.40	0.10	0.08	0.03	0.13
0.50	0.10	0.10	0.00	0.14

**Table 3.** Similar to Table 2, but using the  $\text{NDVI}_{\infty}$  and  $\text{NDVI}_0$  values extracted from the ASTER spectral library.

NDVI	$d_{\text{NDVI}}$	$d_{\text{NDVI}\%}$	$d_{\text{NDVI}0}$	$e(\text{FVC})$
0.2	0.08	0.00	0.08	0.11
0.3	0.08	0.01	0.07	0.11
0.4	0.08	0.03	0.05	0.10
0.5	0.08	0.04	0.04	0.10
0.6	0.08	0.05	0.03	0.10
0.7	0.08	0.07	0.01	0.11
0.8	0.08	0.08	0.00	0.12

Despite the NDVI has been widely used for assessment and monitoring of changes in canopy biophysical properties such FVC, this vegetation index shows problems of saturation for high vegetation covers, as has been pointed out by [13]. The authors found that for FVC higher than 60% the NDVI is almost insensitive to FVC changes, mainly due to the NIR reflectance behaviour. In order to solve this problem and using the concept of ARVI (Atmospherically Resistant Vegetation Index) [14], [12] propose an empirical relationship between FVC and a new index denoted as  $\text{VARI}_{\text{green}}$  (Variable Atmospherically Resistant Index) and given by:

$$\text{VARI}_{\text{green}} = \frac{\mathbf{r}_{\text{green}} - \mathbf{r}_{\text{red}}}{\mathbf{r}_{\text{green}} + \mathbf{r}_{\text{red}} - \mathbf{r}_{\text{blue}}} \quad (9)$$

The expression of the  $\text{VARI}_{\text{green}}$  is similar to the NDVI (Equation 1), but substituting the NIR reflectance by the

green reflectance ( $\rho_{\text{green}}$ ) and including the blue reflectance ( $\rho_{\text{blue}}$ ) in order to compensate the atmospheric effects. Despite TOA (Top Of Atmosphere) reflectances can be also used in order to calculate the NDVI, better results can be achieved by using at-surface or atmospherically corrected reflectances. However,  $\text{VARI}_{\text{green}}$  is calculated using TOA reflectances, so the atmospheric correction is included in Equation (9) by means of the blue reflectivity. Using 71 samples [12] obtained the following linear relationship between FVC and VARI:

$$\text{FVC}(\%) = 84.75\text{VARI}_{\text{green}} + 22.78 \quad (10)$$

with a standard error of estimation less than 10%.

### 3.2. Spectral Mixture Analysis

The Spectral Mixture Analysis (SMA) technique has been developed in recent years to extract land-cover information at a sub-pixel level. SMA divides each ground resolution element into its constituent materials using endmembers (EMs), which represent the spectral characteristics of the cover types. When applied to multispectral satellite data, the result is a series of images each depicting the abundance of a cover type. The basic physical assumption is that there is not a significant amount of photon multiple scattering between the macroscopic materials, in such a way that the flux received by the sensor represents a summation of the fluxes from the cover types (macroscopic materials) and the fraction of each one is proportional to its covered area [5]. This assumption complies with the properties of the considered CHRIS/PROBA data sets, collected over a flat area and dominated by homogeneous crop fields. As a result, most of the endmember substances are sitting side-by-side within the field of view of the imager, and minimal secondary reflections or multiple scattering effects can be assumed. In this paper a simple linear mixing model LSU (Linear Spectral Unmixing) has been used, in which only a few EMs are used to describe the surface composition in each pixel of an image [15]. The reflectivity spectra for each endmember have been automatically extracted from the image using the AMEE (Automated Morphological Endmember Extraction) method. The input to AMEE method is the full spectral data cube, with no previous dimensionality reduction. The method is based on two parameters: a minimum  $S_{\text{min}}$  and a maximum  $S_{\text{max}}$  spatial kernel size. Firstly, a minimum kernel  $K = S_{\text{min}}$  is considered. This structuring element (SE) is moved through all the pixels of the image, defining a spatial context around each hyperspectral pixel [16]. A morphological eccentricity index (MEI) [17] is then obtained by calculating the SAD distance between the two above

signatures. This operation is repeated for all the pixels in the scene, using SEs of progressively increased size, and the resulting scores are used to evaluate each pixel in both spatial and spectral terms. The algorithm performs as many iterations as needed until  $K = S_{\max}$ . The associated MEI value of selected pixels at subsequent iterations is updated by means of newly obtained values, as a larger spatial context is considered, until a final MEI image is generated. Endmember selection is performed by a fully automated approach consisting of two steps: 1) autonomous segmentation of the MEI image, and 2) spatial/spectral growing of resulting regions [16].

### 3.3. Algorithms testing

The expressions shown in section 3.1 have been tested by comparing the estimated values and the ones measured in situ according to the methodology explained in section 2. For this purpose the PROBA/CHRIS image acquired at near nadir view (27.60°) has been used in order to extract the pixel values included in each plot. As has been commented before, in order to obtain FVC from the scaled NDVI is necessary to establish the values of  $NDVI_0$  and  $NDVI_{\infty}$ . Values proposed by [11] or [18] are very useful for global studies, but they could not be appropriate for a particular agricultural area, as is the case of the Barrax test site. In order to estimate the FVC from NDVI values over the Barrax test site, a linear relationship between the NDVI values extracted from the PROBA/CHRIS image and the FVC measured in situ has been obtained:

$$FVC = 1.1101NDVI - 0.0857 \quad (11)$$

with a correlation coefficient  $r = 0.91$  and a standard error of estimation of 13%. The  $NDVI_0$  and  $NDVI_{\infty}$  values can be obtained from Equation (11) by choosing  $FVC = 0$  and  $FVC = 1$ , respectively. In this way one obtains  $NDVI_0 = 0.08$  and  $NDVI_{\infty} = 0.98$ , which agrees with the results obtained by [19] over the same test site. These values lead to an error on FVC less than 8%, according to the sensitivity analysis carried out in section 3.1. The root square addition between this result and the standard error of estimation leads to a final error of 15%.

The direct application of Equation (10), in which FVC is obtained from  $VARI_{\text{green}}$  values as suggested by [13], does not provides good results and tends to underestimate de FVC in comparison with the in situ values, with a root mean square error of 28%, which can be explained by taking into account that Equation (10) was obtained over a particular area. Recalculating this expression according to the FVC values measured in situ and the  $VARI_{\text{green}}$  values extracted from the CHRIS data, it is possible to obtain:

$$FVC(\%) = 113.30VARI_{\text{green}} + 43.40 \quad (12)$$

with a correlation coefficient  $r = 0.97$  and a standard error of estimation of 8%, in more accordance with the results obtained by [13].

In order to obtain the FVC applying a LSU technique the AMEE method described in section 3.2 has been used in order to extract the EMs from the image without a priori knowledge of the field site. The AMEE method extracted a total amount of 10 EMs, in which 2 EMs for green vegetation have been found (the rest of the EMs correspond to clouds, shadows, bare soil, etc.). The comparison with in situ measurements shows a final root mean square error (RMSE) less than 12% is obtained. The LSU has been also applied using only 2 EMs (bare soil and green vegetation) extracted from the image by using the land cover map of the field site. In this way the results are slightly better, with a RMSE less than 9%. The main constraint in this case is that a priori knowledge of the field site is needed in order to extract the EMs.

According to the results obtained, FVC can be retrieved from satellite data using a linear relationship with the NDVI, with errors lower than 15%, and using a linear relationship with the  $VARI_{\text{green}}$ , improving in this way the results, with errors lower than 10%. FVC can be also obtained using a LSU method and automatically extracted EMs, i.e., without a prior knowledge of the field site. In this way, errors lower than 12% are obtained.

### 4. ANGULAR EFFECTS

In order to analyze the angular effects on the FVC retrieved from satellite data, NDVI and  $VARI_{\text{green}}$  values have been extracted for each plot at the five PROBA/CHRIS acquisition view zenith angles: -57.40°, -42.53°, 27.60°, 42.44° and 57.29°. Fig. 3 shows the angular variation of the NDVI extracted from the seven plots considered in this study. Differences between the NDVI at each angle and the NDVI at almost nadir view (27.6°) are generally greater for extreme view angles (-57.4° and 57.3°). Differences are lower than 0.04 in most cases, except for the corn (C1) plot, reaching values of 0.07. These differences are not important when estimating the FVC from NDVI values, as is shown in Fig. 4, in which the FVC estimated from Equation (11) for each observation angle is graphed. Differences lower than 5% are obtained in all cases except for the corn (C1) plot, reaching differences of 8%. An increase on FVC when increasing the view angle is not observed in all cases, as will be expected. This fact could be explained due to the different angular response of the NDVI at backward and forward directions, as has been pointed out by [19].

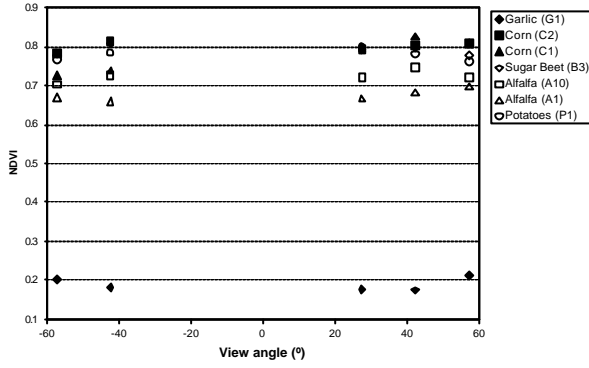


**Fig. 3.** NDVI versus the CHRIS view angle for different samples.

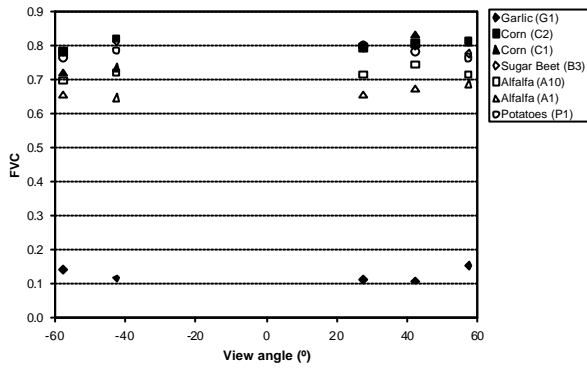


**Fig. 4.** Fractional vegetation cover estimated using a linear relationship with the NDVI versus the CHRIS view angle.

Low variations on NDVI with the view angle has been also obtained by [20]. These authors point out that the higher angular variations on NDVI are due to changes in the solar zenith angle, and not in the view angle. It should be noted that angular variations on NDVI and also FVC are higher for heterogeneous surfaces than for homogeneous ones. In this study the plots selected tend to be homogeneous, with high vegetation cover except for the garlic plot (G1), with very low vegetation cover. So in these cases negligible corrections between the values obtained at each view angle and the nadir one have been obtained. Negligible angular variations has been also observed when analyzing the results obtained with the LSU analysis.

## 5. EMISSIVITY RETRIEVAL FROM FVC VALUES

Land surface emissivity (LSE) is a parameter involved in the thermal part of the spectrum and is a key variable in order to retrieve land surface temperature with a good accuracy over natural surfaces, which are not perfect blackbodies. LSE is also important in

geological studies. Different satellite methods have been published in the last years in order to retrieve LSE from thermal infrared satellite data: the reference channel method [21], thermal spectral indices [22], alpha residuals [23], day/night methods [24], the Temperature and Emissivity Separation (TES) method [25], among others. LSE can be also obtained from visible and near infrared satellite data. These methods estimate LSE from NDVI or FVC values [26,27,18]. In this context, LSE can be obtained for a mixed surface composed by soil and vegetation using the following very simplified parameterization:

$$\mathbf{e} = \mathbf{e}_s(1 - P_v) + \mathbf{e}_v P_v \quad (13)$$

where  $\mathbf{e}_s$  refers to the soil emissivity,  $\mathbf{e}_v$  to the vegetation emissivity and  $P_v$  is the FVC. Equation (13) must be particularized to a certain wavelength or sensor band. In this last case, effective instead of spectral emissivities will be used according to the following expression:

$$\mathbf{e} = \frac{\int \mathbf{e}_l f_l d\mathbf{l}}{\int f_l d\mathbf{l}} \quad (14)$$

where  $f_\lambda$  is the spectral function for a given sensor band or simply filter function. According to error theory, the uncertainty on the emissivity,  $e(\mathbf{e})$ , calculated using Equation (13) is given by

$$e(\mathbf{e}) = \sqrt{\mathbf{d}_{\mathbf{e}_s}^2 + \mathbf{d}_{\mathbf{e}_v}^2 + \mathbf{d}_{P_v}^2} \quad (15)$$

where

$$\mathbf{d}_{\mathbf{e}_s} = \left| \frac{\partial \mathbf{e}}{\partial \mathbf{e}_s} \right| e(\mathbf{e}_s) = (1 - P_v) e(\mathbf{e}_s) \quad (16)$$

$$\mathbf{d}_{\mathbf{e}_v} = \left| \frac{\partial \mathbf{e}}{\partial \mathbf{e}_v} \right| e(\mathbf{e}_v) = P_v e(\mathbf{e}_v) \quad (17)$$

$$\mathbf{d}_{P_v} = \left| \frac{\partial \mathbf{e}}{\partial P_v} \right| e(P_v) = (\mathbf{e}_v - \mathbf{e}_s) e(P_v) \quad (18)$$

and  $e(\mathbf{e}_s)$ ,  $e(\mathbf{e}_v)$  and  $e(P_v)$  refers to the errors on soil emissivity, vegetation emissivity and FVC, respectively.

Therefore, in order to apply Equation (13), effective soil and vegetation emissivities for a certain thermal band are needed. The study will be focused on field thermal radiometers bands, so these instruments are used in order to obtain in situ values. In this case, we will consider two CIMEL radiometers, model CE 312-1 (CIMEL 1), with four bands in the thermal region between 8 and 14  $\mu\text{m}$ , and model CE 312-2 (CIMEL 2),

with six bands in 8-14  $\mu\text{m}$ . It should be noted that both radiometers include a broadband, and the five narrowbands of the model CE 312-2 are in coincidence with the five ASTER (Advanced Spaceborne Thermal Emission and Reflection radiometer) thermal bands, whereas CIMEL 1 bands 3 and 2 are very similar to the AVHRR (Advanced Very High Resolution Radiometer) bands 4 and 5, respectively. Soil and vegetation band emissivities have been obtained applying Equation (14) to each CIMEL band and using the spectra included in the ASTER spectral library (<http://speclib.jpl.nasa.gov>). As an example, the effective values obtained for CIMEL 1 are shown in Table 4. It should be noted that vegetation emissivities show low standard deviations for all CIMEL bands, whereas soil emissivities show only low standard deviations for CIMEL bands included in the region 10-12  $\mu\text{m}$ . Bands included in the region 8-9.5  $\mu\text{m}$  show high standard deviations, so a general value for soil emissivity is not acceptable for these bands. This problem can be solved by considering only the inceptisol class, which is the more common soil class on the Earth's surface and also in the Barrax test site.

**Table 4.** Mean effective emissivities obtained from the ASTER spectral library for the CIMEL 1 radiometer. The standard deviation is shown in brackets.

CLASS	BAND 1	BAND 2	BAND 3	BAND 4
Alfisol	0.950 (0.016)	0.976 (0.003)	0.967 (0.004)	0.912 (0.043)
Aridisol	0.959 (0.012)	0.974 (0.004)	0.969 (0.007)	0.939 (0.027)
Entisol	0.946 (0.021)	0.979 (0.002)	0.969 (0.006)	0.896 (0.058)
Inceptisol	0.962 (0.009)	0.976 (0.004)	0.969 (0.006)	0.946 (0.017)
Mollisol	0.966 (0.009)	0.978 (0.002)	0.972 (0.003)	0.951 (0.020)
<b>All soils</b>	<b>0.957</b> <b>(0.016)</b>	<b>0.976</b> <b>(0.004)</b>	<b>0.969</b> <b>(0.006)</b>	<b>0.928</b> <b>(0.041)</b>
Vegetation	0.983 (0.007)	0.984 (0.010)	0.982 (0.008)	0.982 (0.007)

Table 5 shows the final expressions for emissivity retrieval at-nadir view according to Equation (13). The total error on emissivity according to Equations (15) to (18) versus the FVC value is shown in Fig. 5 for CIMEL 1. The total error has been calculated assuming an error for soil and vegetation emissivities equal to the standard deviation and an error for FVC equal to 10%. For CIMEL 1 bands, the errors are lower than 0.01 except for band 4 (11.96  $\mu\text{m}$ ) with low FVC values.

**Table 5.** Expressions for the land surface emissivity retrieval from fractional vegetation cover ( $P_v$ ) values and for each CIMEL band.

MODEL	BAND	EXPRESSION
CIMEL 1	1 (10.54 $\mu\text{m}$ )	$\epsilon = 0.962 + 0.021 P_v$
	2 (11.96 $\mu\text{m}$ )	$\epsilon = 0.976 + 0.008 P_v$
	3 (10.80 $\mu\text{m}$ )	$\epsilon = 0.969 + 0.013 P_v$
	4 (8.82 $\mu\text{m}$ )	$\epsilon = 0.946 + 0.036 P_v$
CIMEL 2	1 (10.54 $\mu\text{m}$ )	$\epsilon = 0.962 + 0.021 P_v$
	2 (11.29 $\mu\text{m}$ )	$\epsilon = 0.970 + 0.013 P_v$
	3 (10.57 $\mu\text{m}$ )	$\epsilon = 0.968 + 0.013 P_v$
	4 (9.15 $\mu\text{m}$ )	$\epsilon = 0.941 + 0.038 P_v$
	5 (8.69 $\mu\text{m}$ )	$\epsilon = 0.949 + 0.033 P_v$
	6 (8.43 $\mu\text{m}$ )	$\epsilon = 0.946 + 0.040 P_v$

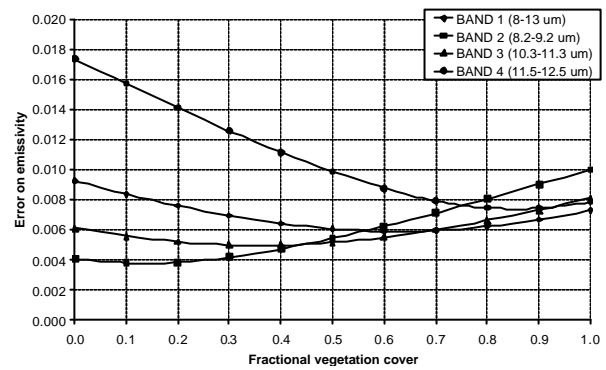


**Fig. 5.** Total error on emissivity versus the fractional vegetation cover for CIMEL 1 bands.

As an example, Figure 6 shows the land surface emissivity map obtained for the CIMEL broadband (8-13  $\mu\text{m}$ ) and using the FVC image obtained with the LSU technique.

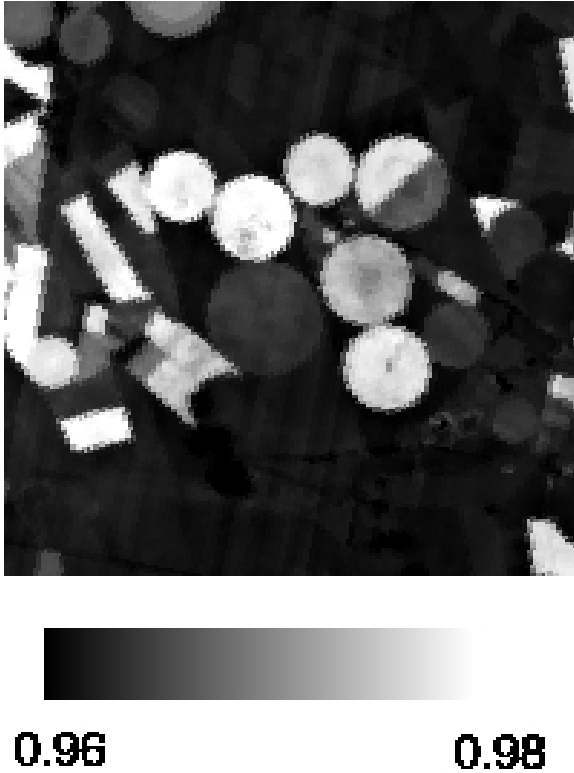


**Fig. 6.** Land surface broadband (8-13  $\mu\text{m}$ ) emissivity map obtained from CHRIS data over the Barrax test site (see land use map in Figure 3).

Before ending this section, a comment about the validity of Equation (13) for surface emissivity retrieval should be given. Hence, Equation (13) is only valid for flat surfaces. For rough surfaces the cavity effect should be taken into account, for example in the following way:

$$\mathbf{e} = \mathbf{e}_s(1 - P_v) + \mathbf{e}_v P_v + C \quad (19)$$

where the term  $C$  includes the cavity effect. Following the methodology proposed by [28], the term  $C$  can be obtained by geometrical considerations applied to crops distributed in rows. Therefore, it is difficult to obtain the cavity term from satellite data. Reference [29] give a constant value for a cavity term, not depending on the LAI (Leaf Area Index) or FVC value, which could not be true in all cases. The retrieval of the cavity term from satellite data is not an easy task and requires further research. For this reason it has not been included in this paper. Anyway, when the cavity effect could be evaluated (for example from in situ measurements), it should be added to the emissivity value retrieved from Equation (13). Additional discussion about the validity of Equation (13) can be found in [30].

## 6. CONCLUSIONS

The fraction of vegetation cover or FVC is a key variable in many environmental studies. Different approaches have been published in order to retrieve this parameter from satellite data. Traditionally, these approaches have used relations between FVC and vegetation indices. In this paper relationships between the FVC and the NDVI and VARI indices adapted for CHRIS data have been analyzed and tested. Both relations provide good results, especially the FVC vs VARI approach, with errors lower than 10%. This approach has also the advantage of using TOA (Top Of Atmosphere) data, so the atmospheric correction is not needed. The availability of several spectral bands allows the application of other techniques for FVC retrieval, as for example the Spectral Mixture Analysis or, more specifically, the Linear Spectral Unmixing. This technique has been applied using the AMEE method for extracting the endmembers, with error lower than 12%. The results slightly improve when extracting the endmembers from the image with a priori knowledge of the field site, with errors in this case lower than 10%.

Angular effects on vegetation indices and FVC have been also analyzed. The results show low variations on NDVI with view angle, also leading to low angular variations when estimating the FVC from NDVI and also with the other techniques. These low angular variations could be explained taking into account that the samples used in the study have high cover. Moreover, high angular variations on NDVI due to a change on the illumination angle, and not in the view angle, are expected.

Finally, the retrieved FVC has been used for estimating the land surface temperature with a very simplified approximation, in which the emissivity is obtained from soil and vegetation emissivities averaged according to the respective proportion (see Equation 13). When FVC is obtained with an accuracy of 10%, land surface emissivity can be retrieved with an accuracy less than 0.01 in most cases. The main problem with this approximation is the cavity effect, which has not been taken into account. Therefore, for rough surfaces higher errors will be expected. This problem could be solved by including a cavity term in the expression proposed (see Equation 19), but the estimation of the cavity term from remote sensing data needs further research. According to the procedure shown in the paper, land surface emissivity, which is a parameter used when working with thermal infrared data, can be retrieved only using visible and near infrared data. In this way, emissivity maps are obtained from sensors without available thermal bands.

## ACKNOWLEDGEMENTS

The authors wish to thank to the European Union (EAGLE, project SST3-CT-2003-502057) and the Ministerio de Ciencia y Tecnología (project REN2001-3105/CLI) for the financial support. This work has been carried out while Juan C. Jiménez-Muñoz was having a contract “V segles” from the University of Valencia. Also, the authors want to thank Luis Alonso, from the University of Valencia, for his assistance with PROBA/CHRIS geometrical issues.

## REFERENCES

1. Weiss, M., & Baret, F. (1999). Evaluation of canopy biophysical variable retrieval performances from the accumulation of large swath satellite data, *Remote Sensing of Environment*, 70, 293-306.
2. Avissar, R., & Pielke, R. A. (1989). A parameterization of heterogeneous land surfaces for atmospheric numerical models and its impact on regional meteorology, *Monthly Weather Review*, 117, 2113-2136.
3. Trimble, S. W. (1990). Geomorphic effects of vegetation cover and management: some time and space considerations in prediction of erosion and sediment yield, in *Vegetation and Erosion*, edited by J. B. Thornes, London, John Wiley & Sons, pp. 55-66.
4. Smith, M. O., Adams, J. B., & Sabol, D. E. (1994). Spectral mixture analysis: new strategies for the analysis of multispectral data, In *Imaging Spectrometry – A Tool for Environmental Observations*, Euro Courses, Remote Sensing, edited by J. Hill and J. Megier, Dordrecht, Kluwer Academic, Vol. 4, pp. 125-143.
5. Camacho-De Coca, F., García-Haro, F. J., Gilabert, M. A., & Meliá, J. (2004). Vegetation cover seasonal changes assessment from TM imagery in a semi-arid landscape, *International Journal of Remote Sensing*, 25(17), 3451-3476.
6. Barnsley, M. J., Settle, J. J., Cutter, M., Lobb, D., & Teston, F. (2004). The PROBA/CHRIS mission: a low-cost smallsat for hyperspectral, multi-angle, observations of the Earth surface and atmosphere, *IEEE Transactions on Geoscience and Remote Sensing*, 42, 1512-1520.
7. Moreno, J., et al. (2004). The SPECTRA Barrax Campaign (SPARC): Overview and first results from CHRIS data, *Proceedings of 2nd CHRIS/PROBA Workshop*, Frascati, Italy, ESA-ESRIN.
8. Cutter, M. (2004). Review of aspects associated with the CHRIS calibration, *Proceedings of 2nd CHRIS/PROBA Workshop*, Frascati, Italy, ESA-ESRIN.
9. Guanter, L., Alonso, L., & Moreno, J. (2005). Atmospheric Correction Algorithm for CHRIS/PROBA Data over Land. Application to ESA SPARC Campaigns, *Remote Sensing of Environment* (submitted).
10. Martínez, B., Baret, F., Camacho-de Coca, F., García-Haro, F. J., Verger, A., & Meliá, J. (2004). Validation of MSG vegetation products Part I. Field retrieval of LAI and FVC from hemispherical photographs, In *Remote Sensing for Agriculture, Ecosystem and Hydrology*, edited by M. Owe, G. D'Urso, B.T.Gouweleeuw, A.M. Jochum, Vol. 5568, Bellingham, WA, pp. 57-68.
11. Gutman, G., & Ignatov, A. (1998). The derivation of the green vegetation fraction from NOAA/AVHRR data for use in numerical weather prediction models, *International Journal of Remote Sensing*, 19(8), 1533-1543.
12. Carlson, T. N., & Ripley, D. A. (1997). On the relation between NDVI, fractional vegetation cover, and leaf area index, *Remote Sensing of Environment*, 62, 241-252.
13. Gitelson, A. A., Kaufman, Y. J., Stark, R., & Rundquist, D. (2002). Novel algorithms for remote sensing estimation of vegetation fraction, *Remote Sensing of Environment*, 80, 76-87.
14. Kaufman, Y. J., & Tanre, D. (1992). Atmospherically resistant vegetation index (ARVI) for EOS-MODIS, *IEEE Transactions on Geoscience and Remote Sensing*, 30, 261-270.
15. Sabol, D. E., Gillespie, A. R., Adams, J. B., Smith, M. O., & Tucker, C. J. (2002). Structural stage in Pacific Northwest forests estimated using simple mixing models of multispectral images, *Remote Sensing of Environment*, 80, 1-16.
16. Plaza, A., Martínez, P., Pérez, R., & Plaza, J. (2002). Spatial/spectral endmember extraction by multidimensional morphological operations, *IEEE Transactions on Geoscience and Remote Sensing*, 40(9), 2025-2041.

17. Plaza, A., Martínez, P., Pérez, R., & Plaza, J. (2004). A quantitative and comparative analysis of endmember extraction algorithms from hyperspectral data, *IEEE Transactions on Geoscience and Remote Sensing*, 42(3), 650-663.
18. Sobrino, J. A., & Raissouni, N. (2000). Toward remote sensing methods for land cover dynamic monitoring: application to Morocco, *International Journal of Remote Sensing*, 21(2), 353-366.
19. Vercher, A., Camacho de Coca, F., & Meliá, J. (2004). Influencia de la geometría de adquisición en el NDVI, *Revista de Teledetección*, 21, 95-99.
20. Galvao, L. S., Ponzoni, F. J., Epiphanyo, J. C. N., Rudorff, B. F. T., & Formaggio, A. R. (2004). Sun and view angle effects on NDVI determination of land cover types in the Brazilian Amazon region with hyperspectral data, *International Journal of Remote Sensing*, 25(10), 1861-1879.
21. Kahle, A. B., Madura, D. P., & Soha, J. M. (1980). Middle infrared multispectral aircraft scanner data analysis for geological applications, *Applied Optics*, 19, 2279-2290.
22. Becker, F., & Li, Z.-L. (1990). Temperature-independent spectral indices in thermal infrared bands, *Remote Sensing of Environment*, 32, 17-33.
23. Kealy, P. S., & Hook, S. (1993). Separating temperature and emissivity in the thermal infrared multispectral scanner data: Implications for recovering land surface temperature, *IEEE Transactions on Geoscience and Remote Sensing*, 31(6), 1155-1164.
24. Goïta, K., & Royer, A. (1997). Surface temperature and emissivity separability over land surface from combined TIR and SWIR AVHRR data, *IEEE Transactions on Geoscience and Remote Sensing*, 35(3), 718-733.
25. Gillespie, A., Rokugawa, S., Matsunaga, T., Cothorn, J. S., Hook, S., & Kahle, A. B. (1998). A temperature and emissivity separation algorithm for advanced spaceborne thermal emission and reflection radiometer (ASTER) images, *IEEE Transactions on Geoscience and Remote Sensing*, 36, 1113-1126.
26. Van de Griend, A. A., & Owe, M. (1993). On the relationship between thermal emissivity and the normalized difference vegetation index for natural surfaces, *International Journal of Remote Sensing*, 14(6), 1119-1131.
27. Valor, E., & Caselles, V. (1996). Mapping land surface emissivity from NDVI: application to European, African and South American areas, *Remote Sensing of Environment*, 57, 167-184.
28. Sobrino, J. A., Caselles, V., & Becker, F. (1990). Significance of the remotely sensed thermal infrared measurements obtained over a citrus orchard, *ISPRS Photogrammetric Engineering and Remote Sensing*, 44, 343-354.
29. François, C., Ottlé, C., & Prévot, L. (1997). Analytical parametrisation of canopy emissivity and directional radiance in the thermal infrared: Application on the retrieval of soil and foliage temperatures using two directional measurements, *International Journal of Remote Sensing*, 12, 2587-2621.
30. François, C. (2002). The potential of directional radiometric temperatures for monitoring soil and leaf temperature and soil moisture status, *Remote Sensing of Environment*, 80, 122-133.